THE JOURNAL OF PHYSICAL CHEMISTRY B
A JOURNAL OF THE AMERICAN CHEMICAL SOCIETY

pubs.acs.org/JPCB

Article

Manipulating Frontal Polymerization and Instabilities with Phase-Changing Microparticles

Yuan Gao, Mason A. Dearborn, Sagar Vyas, Aditya Kumar, Julie Hemmer, Zhao Wang, Qiong Wu, Omar Alshangiti, Jeffrey S. Moore, Aaron P. Esser-Kahn,* and Philippe H. Geubelle*

Cite This: *J. Phys. Chem. B* 2021, 125, 7537−7545

Read Online

ACCESS | Metrics & More | Article Recommendations | Supporting Information

ABSTRACT: Recently presented as a rapid and eco-friendly manufacturing method for thermoset polymers and composites, frontal polymerization (FP) experiences thermo-chemical instabilities under certain conditions, leading to visible patterns and spatially dependent material properties. Through numerical analyses and experiments, we demonstrate how the front velocity, temperature, and instability in the frontal polymerization of cyclooctadiene are affected by the presence of poly(caprolactone) microparticles homogeneously mixed with the resin. The phase transformation associated with the melting of the microparticles absorbs some of the exothermic reaction energy generated by the FP, reduces the amplitude and order of the thermal instabilities, and suppresses the front velocity and temperatures. Experimental measurements validate predictions of the dependence of the front velocity and temperature on the microparticle volume fraction provided by the proposed homogenized reaction−diffusion model.

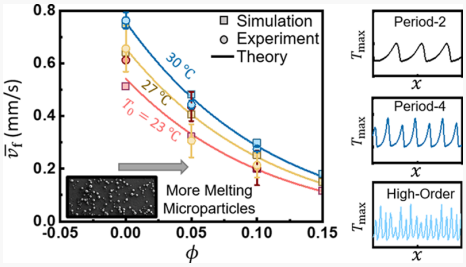

INTRODUCTION

Recently introduced as a rapid, energy-efficient, eco-friendly, out-of-autoclave alternative to conventional bulk-polymerization-based manufacturing for thermoset composites,[1] frontal polymerization (FP) is based on the self-sustaining process associated with the propagation of a sharp polymerization front driven by the exothermic reaction taking place in the thermosetting resin.[2−5]

The key features of the FP-based manufacturing process, including the front temperature and velocity, are sensitive to many factors, including the formulation of the resin,[6−11] the presence of a thermally conductive reinforcing phase,[12−15] the environmental temperature,[16−18] and pressure.[19,20] All of these factors have been shown to affect the morphology and properties of the resultant polymer.[21−24]

In most cases, the polymerization front propagates in a steady fashion, leading to the manufacturing of polymeric materials with homogeneous properties. However, under certain conditions,[25−27] thermo-chemical instabilities are observed in the front propagation, characterized by highly transient front temperatures and velocities. These instabilities have been reported in previous studies as pulsating,[28−30] spinning,[2,31,32] and fingering instabilities.[33] The ultimate objective of this work is to harness these thermal instabilities by changing the process conditions through the tuning of the reaction and thermal transport, leading to spontaneous and controllable patterns and spatially dependent morphological, chemical, optical, and mechanical properties in the polymer.[34]

The numerical and experimental study presented hereafter has two main goals: (1) to investigate how the introduction of microparticles with a melting temperature below the front temperature affects the front velocity and temperature in the FP of cyclooctadiene (COD) through the conversion of some of the reaction heat into energy absorbed by the phase-transforming microparticles; and (2) to show how the amplitude and wavelength of FP-driven thermal instabilities can be tuned by the presence of phase-transforming microparticles, thereby providing a potential methodology to achieve patterning in thermoset polymers and composites. Poly(caprolactone) (PCL) with a combination of proper melting point ∼60 °C, large melting enthalpy 139 J/g, and high compatibility with the COD is expected to interact with the polymerizing front effectively and hence selected as the demonstrative phase-transforming material in the present study. The effects of the environmental temperature and the volume fraction of microparticles on the front velocity and temperature are investigated through a one-dimensional (1D) parametric numerical study, whose results are confirmed by theoretical predictions and experimental observations. In particular, we show how heat absorption associated with

Received: April 30, 2021
Revised: June 14, 2021
Published: July 6, 2021

phase-transforming microparticles reduces the amplitude, wavelength, and order of the pulsating instabilities and describe this effect in terms of a reduction of the Zeldovich number[35] used in previous studies to characterize the onset and order of FP-driven instabilities.

COMPUTATIONAL AND EXPERIMENTAL METHODS

Modeling of FP in the Presence of Phase-Changing Microparticles. *FP in Neat COD Resin.* FP in a neat COD resin (denoted hereafter by the subscript r) in a two-dimensional (2-D) domain can be described by the following reaction−diffusion partial differential equations (PDEs) written in terms of the temperature T (in K) and degree of cure α (nondimensional) fields

$$\begin{cases} \kappa_r \dfrac{\partial^2 T}{\partial x^2} + \kappa_r \dfrac{\partial^2 T}{\partial y^2} + \rho_r H_r \dfrac{\partial \alpha}{\partial t} = \rho_r C_{p,r} \dfrac{\partial T}{\partial t} \\ \dfrac{\partial \alpha}{\partial t} = A_r \exp\left(-\dfrac{E_r}{RT}\right)(1-\alpha)^n \alpha^m \end{cases} \quad (1)$$

In eq 1, κ_r (in W/(m·K)), $C_{p,r}$ (in J/(kg·K)), and ρ_r (in kg/m^3), respectively, denote the thermal conductivity, heat capacity, and density of COD and are listed in the first row of Table 1,[34,36] while H_r (in J/kg) is the amount of heat generated by the exothermic reaction of the resin. The second relation approximates the cure kinetics of COD written with the generalized Prout−Tompkins model,[34] with A_r (in/s), E_r (in J/mol), and R (= 8.314 J/(mol·K)), respectively, denoting the pre-exponential factor, activation energy, and ideal gas constant. n and m correspond to the reaction order. These parameters are summarized in the first row of Table 2.

Table 1. Thermal Conductivity, Density, and Heat Capacity of COD and PCL[34,36]

	κ (W/(m·K))	ρ (kg/m^3)	C_p (J/(kg·K))
COD resin (r)	0.133	882.0	1838.5
PCL particles (p)	0.140	1145	1409.5

The $C_{p,p}$ variation in PCL caused by the phase transition is not considered.

Table 2. Parameters Approximating the Cure Kinetics of COD in eq 1 and the Melting Kinetics of PCL in eq 3[34,37]

	A (1/s)	E(J/mol)	H (J/kg)	n	m
COD resin (r)	2.13×10^{19}	132 000	220 596	2.51	0.82
PCL particles (p)	4.94×10^{35}	241 000	139 000		

To simulate the positive x-direction FP in the domain $0 \le x \le l$, $0 \le y \le w$, we adopt the following initial and boundary conditions

$$\begin{cases} T(x,y,0) = T_0, & 0 \le x \le l, \quad 0 \le y \le w \\ \alpha(x,y,0) = \alpha_0, & 0 \le x \le l, \quad 0 \le y \le w \\ T(0,y,t) = T_{trig}, & 0 \le y \le w, \quad 0 \le t \le t_{trig} \\ \dfrac{\partial T}{\partial x}(0,y,t) = 0 & 0 \le y \le w, \quad t > t_{trig} \end{cases} \quad (2)$$

where T_0 (set at 23 °C), α_0 (= 0.01), T_{trig} (= 175 °C), and t_{trig} (= 5 s), respectively, denote the initial temperature, the initial degree of cure, the triggering temperature, and the triggering time. Adiabatic boundary conditions are applied at all other boundaries. The multiphysics object-oriented simulation environment (MOOSE),[38] an open-source C++ finite element solver that incorporates robust mesh and time step adaptivity modules needed to capture the sharp gradients in the vicinity of the moving front, is adopted in the simulations described hereafter.

Figure 1a presents thermal and degree-of-cure solutions along the front propagating x-direction at different times t, with the temperature T normalized as $\theta = \frac{T - T_0}{T_f - T_0}$, where $T_f = T_0 + \frac{H_r(1-\alpha_0)}{C_{p,r}}$ denotes the "stable" temperature behind the front. The profiles of temperature and degree of cure show the presence of thermal instabilities leading to substantial thermal spikes ($\theta > 1$) as shown in the inset. Since the chemical reaction is driven by the Arrhenius term in the cure kinetics model described by eq 1, the thermal front is always slightly ahead of the degree-of-cure front.

As shown in Figure 1b, these thermal instabilities are also associated with a complex pulsating evolution of the width of the thermal front defined by $L_\theta = \max(\theta)/\max(d\theta/dx)$[17] around its average value $\overline{L_\theta} = 0.29$ mm denoted by the solid horizontal line.

Discrete and Homogenized Models of FP in COD Mixed with PCL Microparticles. We investigate the applicability of a homogenized model of FP in nano-particle-filled COD by performing first a set of simulations of FP in a domain composed of discrete PCL particles of increasingly smaller size embedded in a COD resin (Figure 2a).

The solution in discrete phase-changing PCL particles (denoted hereafter with the subscript p) is obtained with the aid of the following melting−diffusion model describing the evolution of the degree of melting δ

$$\begin{cases} \kappa_p \dfrac{\partial^2 T}{\partial x^2} + \kappa_p \dfrac{\partial^2 T}{\partial y^2} - \rho_p H_p \dfrac{\partial \delta}{\partial t} = \rho_p C_{p,p} \dfrac{\partial T}{\partial t} \\ \dfrac{\partial \delta}{\partial t} = A_p \exp\left(-\dfrac{E_p}{RT}\right)(1-\delta) \end{cases} \quad (3)$$

In the first equation, H_p denotes the melting enthalpy and the negative sign reflects the endothermic nature of the melting process. The second equation approximates the phase transition of the PCL as a first-order kinetic model, where A_p and E_p, respectively, stand for the pre-exponential constant and the activation energy of the melting process.[37,39] The thermal properties and melting kinetics parameters are listed in Tables 1 and 2, respectively.

Equations 1 in the COD resin and eq 3 in the part of the domain occupied by the embedded PCL particles are solved in the rectangular domain shown schematically in Figure 2a while maintaining the particle volume fraction ϕ fixed ($\phi = 0.1$). The discrete model simulations involve a domain length $l = 20$ mm and three pairs of particle radius r and domain width w values (given in mm): $(r, w) = (0.125, 1)$, $(0.0625, 0.5)$, and $(0.03125, 0.25)$. The evolution of the front location x_f defined as the location where $\alpha = 0.5$ along the mid-line (dashed horizontal line ($y = 0.5\ w$) in Figure 2a) is shown in Figure 2b, with the particle radius normalized by the average front width

https://doi.org/10.1021/acs.jpcb.1c03899
J. Phys. Chem. B 2021, 125, 7537−7545

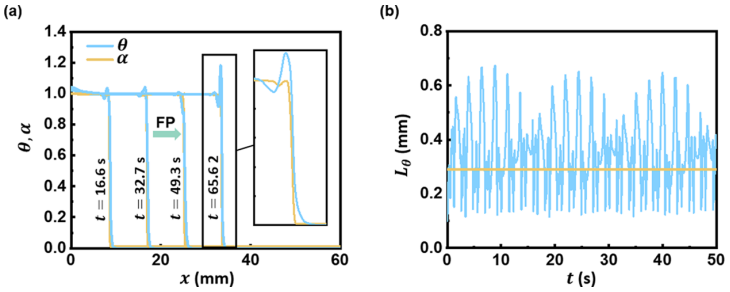

Figure 1. Frontal polymerization of COD. (a) Profiles of normalized temperature θ and degree of cure α at several moments during the right-traveling propagation of the polymerization front. (b) Pulsating evolution of the width L_θ of the thermal front, with the horizontal line denoting the average value $\overline{L_\theta}$.

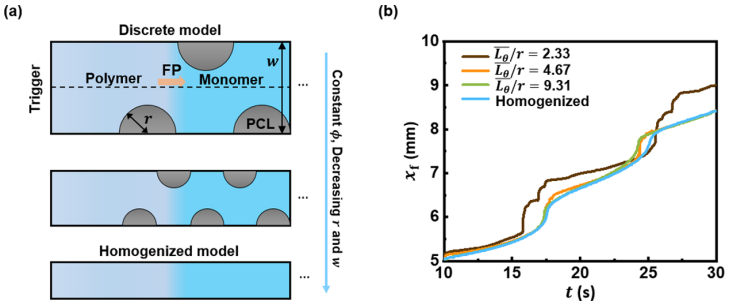

Figure 2. Discrete and homogenized models of FP in COD with PCL particles. (a) Schematics of discrete and homogenized models. (b) Comparison between the evolution of the front position x_f predicted by discrete and homogeneous models.

$\overline{L_\theta}$ introduced in Figure 1b. The initial degree of melting δ_0 is set as 0.01.

As apparent in Figure 2b, the predicted evolution of the front location becomes independent of the particle size when particles become smaller than about 20% of the front width. This result suggests the introduction of a homogenized reaction−melting−diffusion model that simultaneously captures the energy created by the exothermic polymerization of the resin and the energy absorbed by the homogeneously mixed microparticles as

$$\begin{cases} \overline{\kappa}\dfrac{\partial^2 T}{\partial x^2} + (1-\phi)\rho_r H_r \dfrac{\partial \alpha}{\partial t} - \phi\rho_p H_p \dfrac{\partial \delta}{\partial t} = \overline{\rho C_p}\dfrac{\partial T}{\partial t} \\ \dfrac{\partial \alpha}{\partial t} = A_r \exp\left(-\dfrac{E_r}{RT}\right)(1-\alpha)^n \alpha^m \\ \dfrac{\partial \delta}{\partial t} = A_p \exp\left(-\dfrac{E_p}{RT}\right)(1-\delta) \end{cases} \tag{4}$$

The overbar quantities denote the homogenized material properties defined by

$$\begin{cases} \overline{\rho C_p} = \rho_r C_{p,r}(1-\phi) + \rho_p C_{p,p}\phi \ \text{(Rule of mixture)} \\ \overline{\kappa} = \kappa_r + \dfrac{3\kappa_r \phi}{\left(\dfrac{\kappa_p + 2\kappa_r}{\kappa_p - \kappa_r}\right) - \phi} \ \text{(Maxwell model)} \end{cases} \tag{5}$$

As shown in Figure 2b, the front propagation predicted by the homogenized model agrees well with that obtained with a discrete model with PCL particles smaller than approximately 20% of the average thickness of the thermal front. This model is thus adopted for all simulation results presented in the remainder of this manuscript.

Experimental Section. *Materials.* 1,5 Cyclooctadiene (COD) was purchased from Millipore-Sigma and was passed through a 1 cm plug of basic alumina to remove the octadecyl 3-(3,5-di-tert-butyl-4-hydroxyphenyl)propionate stabilizer. Poly(vinyl alcohol) (PVA, MW 13 000−23 000, 98% hydrolyzed), Tween-60, second-generation Grubbs catalyst (GC2), phenylcyclohexane, and tributyl phosphite (TBP) inhibitor were purchased from Sigma-Aldrich and used as received without further purification. Poly(caprolactone) (PCL, MW 50 000) powder was purchased from polysciences.

Preparation of PCL Microparticles. The methodology for the microparticle size reduction was adapted from Chen et al.[40] In a typical preparation, 1.0 g of PCL dissolved in 20 mL of methylene chloride composed the oil phase. This oil phase was added dropwise into 200 mL of 3% PVA solution (external aqueous phase) containing 0.05% of Tween-60 and stirred overnight at 700 rpm to form an O/W emulsion and then allow solvent evaporation. Finally, the produced microparticles were collected by centrifugation, washed with distilled water, and lyophilized by freeze-drying to obtain free-flowing powderlike PCL microparticles.

Morphology Observation. The microparticles were dispersed in distilled water and air-dried onto a smooth silicon wafer chip substrate, and observed using a Carl Zeiss Merlin scanning electron microscope (SEM). Particle size distribution was found by computer analysis using FIJI (ImageJ) to be 15.5 ± 6.0 μm (count 212), below the threshold calculated for applicability to the homogeneous model described in the previous section.

https://doi.org/10.1021/acs.jpcb.1c03899
J. Phys. Chem. B 2021, 125, 7537−7545

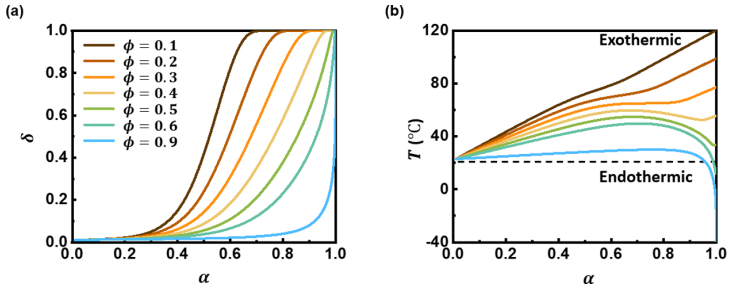

Figure 3. Diffusion-free "bulk polymerization" of the COD/PCL system. Degree of cure α versus degree of melting δ (a) and versus temperature T (b) for different values of the microparticle volume fraction ϕ.

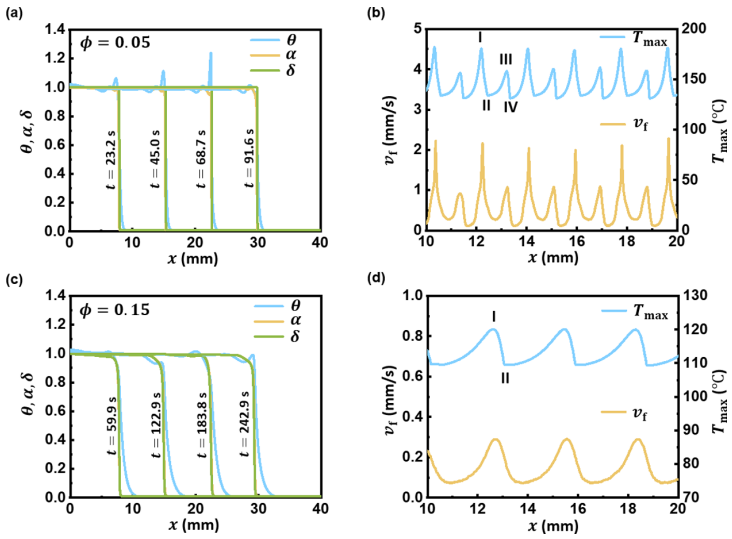

Figure 4. FP in COD with PCL microparticles predicted by the homogenized model. (a, c) Profiles of the normalized temperature θ, the degree of cure α, and the degree of melting δ for ϕ = 0.05 and 0.15. (b, d) Spatial profiles of the instantaneous front velocity v_f and maximum temperature T_{max}.

Frontal Polymerization. In a typical experiment, 3.125 mg of GC2 is weighed out into an Eppendorf tube and dissolved in 156.25 μL of phenylcyclohexane. One molar equivalent of TBP inhibitor with respect to GC2 is added to the solution via a volumetric syringe. Immediately prior to the combination, the PCL microparticles are dispersed in the COD via thorough vortexing and sonication. The catalyst/inhibitor solution is then added to 5 mL of COD (10 000 molar equivalents with respect to GC2) and mixed by inversions. Eight milliliters of the COD-PCL mixture is added to a test tube. A K-type thermocouple (Amprobe TMD-56) is submerged in the mixture to collect data and monitor temperature, which is controlled prior to initiation by submerging the test tube in gently cooled or heated water. Once the target initial temperature is reached, a soldering iron is used to initiate the frontal ring-opening metathesis polymerization (FROMP) reaction at the top of the volume, and the front propagates toward the bottom of the tube.

RESULTS AND DISCUSSION

Numerical Results of Bulk and Frontal Polymerization. The competition between the energy absorbed by the melting of the particles and the energy generated by the exothermic reaction in the COD resin can first be analyzed within the context of bulk polymerization, i.e., in the absence of the thermal diffusion term in eq 4. Results from these so-called "0D simulations" based on the coupled ordinary differential equations (ODEs) for the temperature T, COD degree of cure α, and degree of PCL microparticle melt δ are presented in Figure 3 for the parameter values listed in Tables 1 and 2, and for initial values $(T_0, \alpha_0, \delta_0) = (23\ °C, 0.01, 0.01)$.

Figure 3a compares the evolution of the degree of melting δ with the degree of cure α for seven values of the particle volume fraction ϕ. In all cases, δ remains initially small as α increases, leading to the early increase of the temperature T (Figure 3b). When T approaches the melting temperature of PCL (~60 °C), the phase transformation of the particles is initiated, reflected by a rapid increase of δ and a decrease in the slope of the $T - \alpha$ curves. After the melting is completed (δ = 1), the exothermic reaction in the COD resumes. An increase in ϕ corresponds to a reduction in the available heat of reaction $\rho_r H_r(1 - \phi)$ and an increase in the absorbed heat $\rho_p H_p \phi$ due to the phase transformation of the particles.

As ϕ increases, the initiation of melting thus takes place at higher values of α and the front temperature corresponding to the completion of the curing of COD resin (α = 1) and the melting of PCL (δ = 1) decreases. For this COD/PCL system, the critical value of ϕ for which the available heat of reaction

https://doi.org/10.1021/acs.jpcb.1c03899
J. Phys. Chem. B 2021, 125, 7537−7545

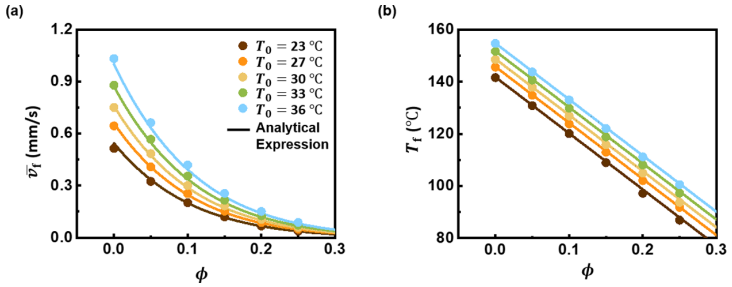

Figure 5. Effect of microparticle volume fraction ϕ and initial temperature T_0 on the average front velocity $\overline{v_f}$ (a) and the front temperature T_f (b). Circles: numerical predictions; curves: analytical expressions with eq 6.

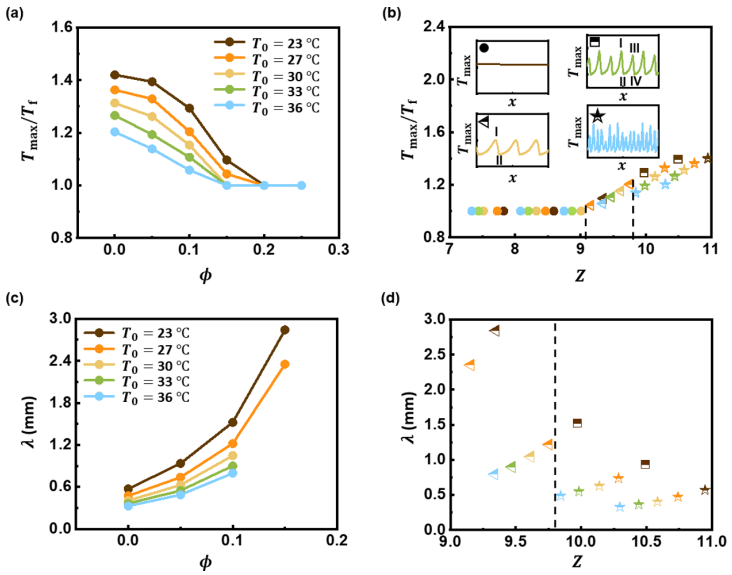

Figure 6. Effect of microparticle volume fraction ϕ and initial temperature T_0 on FP-driven instabilities. Temperature ratio T_{max}/T_f versus (a) ϕ and (b) the Zeldovich number Z for five values of the initial temperature T_0. The insets in (b) show the characteristic T_{max} profile illustrating different modes of front propagation including stable propagation (circles), period-2 instability (triangles), period-4 instability (squares), and higher-order instability (stars). Dependence of the wavelength of instabilities λ on ϕ (c) and Z (d). The significance of the symbols in (d) is the same as in (b).

equals the required heat absorption, i.e., for which $\rho_r H_r(1 - \phi_{crit}) = \rho_p H_p \phi_{crit}$ is found to be $\phi_{crit} = 0.55$. As apparent in Figure 3b, the system will become endothermic for $\phi > \phi_{crit}$.

This simple "0D model" does not capture the sharp gradients present in the vicinity of the front and the contribution of the thermal diffusion process needed to drive the frontal polymerization. To model the impact of PCL microparticles on the propagation of the polymerization front, we solve the system of coupled PDEs described by eq 4 in a 1D domain of length l = 40 mm, with the same thermal trigger in eq 2.

Figure 4a,c presents snapshots of the profiles of temperature, degree of cure, and degree of melting obtained for ϕ = 0.05 and 0.15. For this homogenized model, the normalized temperature is defined as $\theta = \frac{T - T_0}{T_f - T_0}$, with T_f denoting the front temperature obtained by

$$T_f = T_0 + \frac{\rho_r H_r(1 - \phi) - \rho_p H_p \phi}{\overline{\rho C_p}} \quad (6)$$

As before, the thermal front precedes the degree-of-cure front since the cure kinetics is thermally driven. The profile in δ is sharper than that in α indicating that the phase transition, although being driven by the heat of reaction, takes place faster than the polymerization as alluded to in Figure 3a. As apparent in Figure 4c, the thermal front becomes less sharp and the front velocity decreases as the particle volume fraction increases.

The thermal spikes for which $\theta > 1$ confirm the existence of pulsating instabilities, as illustrated in Figure 4b,d, which present the spatial variation of the maximum temperature T_{max} and front velocity v_f along the path of the front. A direct correlation can be observed between the peaks and valleys in T_{max} and v_f. For the case ϕ = 0.05, we obtain a period-4 oscillation marked as I, II, III, and IV in Figure 4b. The solution obtained for ϕ = 0.15 is quite different, with the "repeating unit" of v_f and T_{max} displaying a period-2 oscillation marked by I and II in Figure 4d. Moreover, as further discussed in the next section, the average front velocity and temperature are strongly affected by the particle volume fraction.

https://doi.org/10.1021/acs.jpcb.1c03899
J. Phys. Chem. B 2021, 125, 7537−7545

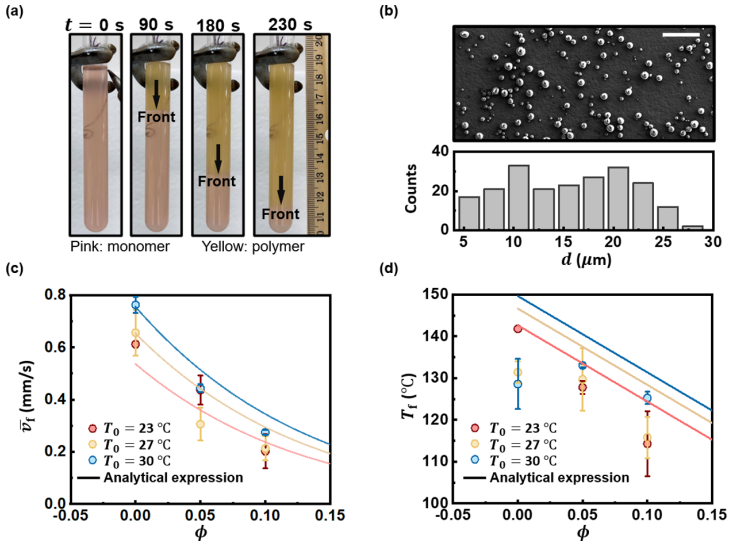

Figure 7. Experiments of FP with PCL microparticles. (a) Optical images of FP with PCL microparticles in a test tube with a volume fraction of microparticles $\phi = 0.1$. The front is propagating downward (black arrows), transforming monomer (in pink) into a polymer (in yellow). (b) SEM image of PCL microparticles with the scale bar representing 100 μm. A size distribution analysis indicates the averaged particle diameter $d = 15.5 \pm 6.0$ μm. (c) Average front velocity $\overline{v_f}$ and (d) front temperature T_f as functions of the microparticle volume fraction ϕ and the initial temperature T_0. The melting enthalpy H_p in analytical models is changed to 89 J/g.

Effects of Initial Temperature and Microparticle Volume Fraction. As shown earlier, the key features (front velocity, temperature, and instabilities) of FP in the COD/PCL system depend on the energy released by the chemical reaction and the amount of heat absorbed by the phase transition. We present hereafter the results of a parametric study on the effects of the microparticle volume fraction and the initial temperature of the resin on these key FP features.

Figure 5a,b present the dependence of the average front velocity $\overline{v_f}$ and of the front temperature T_f on the particle volume fraction ϕ and the initial temperature T_0, with $\overline{v_f}$ computed based on the time needed for the front to travel between $x = 10$ and 30 mm. An increased amount of microparticles rapidly slows down the front and strongly reduces its temperature. Also, as expected, higher values of the initial temperature lead to faster fronts.

The numerical results shown as symbols in Figure 5a can be captured through the following analytical approximation $\tilde{v}_f$ for the front velocity[41−43]

$$V_f = \max_{\varepsilon} \sqrt{\frac{A_r \bar{\kappa}}{\rho_r H_r (1-\phi) - \rho_p H_p \phi} \frac{R\hat{T}(\varepsilon)^2}{E_r} \exp\left(\frac{-E_r}{R\hat{T}(\varepsilon)}\right) \frac{1}{\Pi[m, n, \alpha_0, \varepsilon]}} \tag{7}$$

where $\hat{T}(\varepsilon) = T_0 + \frac{(1-\alpha_0-\varepsilon)(\rho_r H_r(1-\phi) - \rho_p H_p \phi)}{\overline{\rho C_p}}$ is the effective front temperature of the instantaneous energy release, $\Pi[m, n, \alpha_0, \varepsilon] = \int_0^{1-\varepsilon-\alpha_0} \frac{y}{(y+\varepsilon)^n (1-\varepsilon-y)^m} dy$ is a coefficient with a form determined by the general Prout−Tompkins model, and ε between 0 and $1 - \alpha_0$ is the degree of cure at the instantaneous energy release.[43] The analytical values of the front velocity provided by eq 7 (solid curves) agree well with the numerical results (symbols) for all values of T_0. Similarly, Figure 5b shows a good agreement between the numerical values of T_f (symbols) and the analytical expression given by eq 6 (solid curves).

Turning our attention to the relationship between microparticle volume fraction and instabilities, we adopt the temperature ratio T_{max}/T_f (both expressed in K) to quantify the amplitude of thermal instabilities. Figure 6 presents the dependence of the temperature ratio on ϕ and T_0, showing that the addition of phase-changing particles rapidly reduces and eventually eliminates (for $\phi \geq 0.2$) the FP-driven instabilities. In addition, the higher the initial temperature of the resin, the lower the amplitude of the thermal instabilities as was observed in DCPD[27] and methacrylic acid.[44]

A detailed analysis of these results yields three modes of pulsating instabilities as illustrated in the insets of Figure 6b: period-2 instabilities (triangles), period-4 instabilities (squares), and higher-order instabilities (stars). The first inset (circle) shows the stable propagation for reference.

Figure 6b shows how the temperature ratio T_{max}/T_f relates to the Zeldovich number, which has long been used to characterize the onset of instability[26,44,45]

$$Z = \frac{T_f - T_0}{T_f} \frac{E_r}{RT_f} \tag{8}$$

As apparent in that figure, the temperature ratio decreases with Z and pulsating instabilities disappear for $Z < 9.1$. Moreover, for $9.1 < Z < 9.75$, period-2 pulsating instabilities are observed, while period-4 and higher-order instabilities are obtained for $Z > 9.75$. As microparticles suppress the FP-driven instabilities at a higher ϕ, v_f is also significantly reduced on compromise. However, a larger v_f can be maintained at a higher initial temperature T_0 (Figure S1).

Figure 6c focuses on the dependence of the wavelength λ of these instabilities on ϕ and T_0. An increase in particle content leads to an increase in λ, defined as the average distance

https://doi.org/10.1021/acs.jpcb.1c03899
J. Phys. Chem. B 2021, 125, 7537−7545

between adjacent peaks in the maximum temperature profile. The discontinuous dependence of λ on Z presented in Figure 6d corresponds to the aforementioned transitions between instability modes.

Experimental Validation. To verify the numerical findings, experiments of FP with PCL microparticles were performed in test tubes, as exemplified by Figure 7a, where the volume fraction of microparticles $\phi = 0.1$. At $t = 0$ s, a visible front is triggered by a soldering iron, propagating downward at an averaged velocity of ~0.2 mm/s, transforming liquid COD monomers (in pink) to solid polybutadiene (in yellow). After FP, the samples are lacking visible defects. A scanning electron microscope (SEM) photo of PCL microparticles is presented in Figure 7b; the scale bar represents 100 μm. The size distribution analysis indicates that the diameter of PCL microparticles ranges from 4.3 to 29.2 μm with an averaged particle diameter d of 15.5 ± 6.0 μm, which justifies the usage of the homogeneous model in eq 4 (Figure 2b). Differential scanning calorimetry (DSC) measurements are demonstrated in Figure S2, which verify the melting kinetics approximated by eq 3 but indicate a lower H_p of 89 ± 2.0 J/g compared to that of PCL with 100% crystallinity (Table 1).

The instabilities with mm-sized wavelength λ explored with numerical analyses are difficult to directly observe in experiments due to insufficient resolutions and the experimental results presented hereafter focus on the dependence of the front velocity on the particle volume fraction and initial temperature. Figure 7c shows that the average front velocity $\overline{v_f}$ measured in experiments (dots) increases with the initial temperature T_0 but decreases with the volume fraction ϕ of PCL microparticles, as suggested by the numerical results. Moreover, the experimental results of $\overline{v_f}$ are highly consistent with the analytical prediction given by eq 7 (solid lines). According to Figure 7d, the trends of front temperature measured by a thermocouple with T_0 and ϕ generally agree with numerical and analytical findings. However, the experimental value is systematically lower than the analytical prediction given by (eq 6) due to the heat loss to the surroundings,[46] which was not considered in the present modeling work.

CONCLUSIONS

With the aid of numerical analyses and experiments, we have shown how mixing PCL microparticles with a COD resin affects the frontal polymerization process. A homogenized model of the resin/phase-changing particle system has been proposed and shown to be applicable for particle sizes inferior to about 20% of the average thermal front thickness. A parametric study has been carried out to investigate systematically the effects of the microparticle concentration and resin initial temperature on the frontal polymerization of COD, and in particular on the front velocity, temperature, and instability. Good agreement was found between numerical results, theoretical predictions, and experimental observations. These results have illustrated how the FP-driven instabilities can be harnessed by mixing endothermic phase-transforming microparticles, thereby provides a potential path for the efficient manufacturing of polymer and polymeric-matrix composites with controlled patterns and spatially dependent material properties.

ASSOCIATED CONTENT

Supporting Information

The Supporting Information is available free of charge at https://pubs.acs.org/doi/10.1021/acs.jpcb.1c03899.

DSC measurements on PCL microparticles; relationships between instabilities and front velocities (PDF)

AUTHOR INFORMATION

Corresponding Authors

Aaron P. Esser-Kahn − *Pritzker School of Molecular Engineering, University of Chicago, Chicago, Illinois 60637, United States;* orcid.org/0000-0003-1273-0951; Phone: +1(773)834-2948; Email: aesserkahn@uchicago.edu

Philippe H. Geubelle − *Beckman Institute of Advanced Science and Technology and Department of Aerospace Engineering, University of Illinois, Urbana, Illinois 61801, United States;* orcid.org/0000-0002-4670-5474; Phone: +1(217)244-7648; Email: Email: geubelle@illinois.edu

Authors

Yuan Gao − *Beckman Institute of Advanced Science and Technology and Department of Aerospace Engineering, University of Illinois, Urbana, Illinois 61801, United States;* orcid.org/0000-0001-6030-9497

Mason A. Dearborn − *Pritzker School of Molecular Engineering, University of Chicago, Chicago, Illinois 60637, United States*

Sagar Vyas − *Beckman Institute of Advanced Science and Technology and Department of Aerospace Engineering, University of Illinois, Urbana, Illinois 61801, United States*

Aditya Kumar − *Beckman Institute of Advanced Science and Technology and Department of Aerospace Engineering, University of Illinois, Urbana, Illinois 61801, United States*

Julie Hemmer − *Beckman Institute of Advanced Science and Technology, University of Illinois, Urbana, Illinois 61801, United States*

Zhao Wang − *Pritzker School of Molecular Engineering, University of Chicago, Chicago, Illinois 60637, United States*

Qiong Wu − *Beckman Institute of Advanced Science and Technology and Department of Chemistry, University of Illinois, Urbana, Illinois 61801, United States;* orcid.org/0000-0001-8768-7738

Omar Alshangiti − *Beckman Institute of Advanced Science and Technology and Department of Chemistry, University of Illinois, Urbana, Illinois 61801, United States*

Jeffrey S. Moore − *Beckman Institute of Advanced Science and Technology and Department of Chemistry, University of Illinois, Urbana, Illinois 61801, United States;* orcid.org/0000-0001-5841-6269

Complete contact information is available at: https://pubs.acs.org/10.1021/acs.jpcb.1c03899

Notes

The authors declare no competing financial interest.

ACKNOWLEDGMENTS

This work was supported by the U.S. Air Force Office of Scientific Research through Award FA9550-20-1-0194 as part of the Center of Excellence in Self-healing and Morphogenic Manufacturing. The authors also acknowledge the support of

the National Science Foundation for Grant No. 1933932 through the GOALI: Manufacturing USA: Energy Efficient Processing of Thermosetting Polymers and Composites.

REFERENCES

(1) Robertson, I. D.; Yourdkhani, M.; Centellas, P. J.; Aw, J. E.; Ivanoff, D. G.; Goli, E.; Lloyd, E. M.; Dean, L. M.; Sottos, N. R.; Geubelle, P. H.; et al. Rapid Energy-Efficient Manufacturing of Polymers and Composites via Frontal Polymerization. *Nature* **2018**, *557*, 223−227.
(2) Pojman, J. A.; Ilyashenko, V. M.; Khan, A. M. Free-Radical Frontal Polymerization: Self-Propagating Thermal Reaction Waves. *J. Chem. Soc., Faraday Trans.* **1996**, *92*, 2825−2837.
(3) Mariani, A.; Bidali, S.; Fiori, S.; Sangermano, M.; Malucelli, G.; Bongiovanni, R.; Priola, A. UV-Ignited Frontal Polymerization of an Epoxy Resin. *J. Polym. Sci., Part A: Polym. Chem.* **2004**, *42*, 2066−2072.
(4) Frulloni, E.; Salinas, M.; Torre, L.; Mariani, A.; Kenny, J. M. Numerical Modeling and Experimental Study of the Frontal Polymerization of the Diglycidyl Ether of Bisphenol A/Diethylenetriamine Epoxy System. *J. Appl. Polym. Sci.* **2005**, *96*, 1756−1766.
(5) Mariani, A.; Fiori, S.; Chekanov, Y.; Pojman, J. A. Frontal Ring-Opening Metathesis Polymerization of Dicyclopentadiene. *Macromolecules* **2001**, *34*, 6539−6541.
(6) Liu, H.; Wei, H.; Moore, J. S. Frontal Ring-Opening Metathesis Copolymerization: Deviation of Front Velocity from Mixing Rules. *ACS Macro Lett.* **2019**, *8*, 846−851.
(7) Goli, E.; Robertson, I.; Geubelle, P.; Moore, J. S. Frontal Polymerization of Dicyclopentadiene: A Numerical Study. *J. Phys. Chem. B* **2018**, *122*, 4583−4591.
(8) Robertson, I. D.; Pruitt, E.; Moore, J. S. Frontal Ring-Opening Metathesis Polymerization of Exo-Dicyclopentadiene for Low Catalyst Loadings. *ACS Macro Lett.* **2016**, *5*, 593−596.
(9) Alzari, V.; Nuvoli, D.; Scognamillo, S.; Piccinini, M.; Gioffredi, E.; Malucelli, G.; Marceddu, S.; Sechi, M.; Sanna, V.; Mariani, A. Graphene-Containing Thermoresponsive Nanocomposite Hydrogels of Poly (N-isopropylacrylamide) Prepared by Frontal Polymerization. *J. Mater. Chem.* **2011**, *21*, 8727−8733.
(10) Mariani, A.; Fiori, S.; Bidali, S.; Alzari, V.; Malucelli, G. Frontal Polymerization of Diurethane Diacrylates. *J. Polym. Sci., Part A: Polym. Chem.* **2008**, *46*, 3344−3352.
(11) Fiori, S.; Mariani, A.; Ricco, L.; Russo, S. First Synthesis of a Polyurethane by Frontal Polymerization. *Macromolecules* **2003**, *36*, 2674−2679.
(12) Goli, E.; Parikh, N.; Yourdkhani, M.; Hibbard, N.; Moore, J.; Sottos, N.; Geubelle, P. H. Frontal Polymerization of Unidirectional Carbon-Fiber-Reinforced Composites. *Composites, Part A* **2020**, *130*, No. 105689.
(13) Dzhardimalieva, G. I.; Pomogailo, A. D.; Volpert, V. A. Frontal Polymerization of Metal-Containing Monomers: A Topical Review. *J. Inorg. Organomet. Polym.* **2002**, *12*, 1−21.
(14) Mota-Morales, J. D.; Gutiérrez, M. C.; Ferrer, M. L.; Jiménez, R.; Santiago, P.; Sanchez, I. C.; Terrones, M.; Del Monte, F.; Luna-Bárcenas, G. Synthesis of Macroporous Poly(acrylic acid)-Carbon Nanotube Composites by Frontal Polymerization in Deep-Eutectic Solvents. *J. Mater. Chem. A* **2013**, *1*, 3970−3976.
(15) Gary, D. P.; Bynum, S.; Thompson, B. D.; Groce, B. R.; Sagona, A.; Hoffman, I. M.; Morejon-Garcia, C.; Weber, C.; Pojman, J. A. Thermal Transport and Chemical Effects of Fillers on Free-Radical Frontal Polymerization. *J. Polym. Sci.* **2020**, *58*, 2267−2277.
(16) Chechilo, N.; Enikolopyan, N. Effect of Pressure and Initial Temperature of the Reaction Mixture During Propagation of a Polymerization Reaction. *Dokl. Phys. Chem.* **1976**, *230*, 840−843.
(17) Vyas, S.; Goli, E.; Zhang, X.; Geubelle, P. Manufacturing of Unidirectional Glass-Fiber-Reinforced Composites via Frontal Polymerization: A Numerical Study. *Compos. Sci. Technol.* **2019**, *184*, No. 107832.
(18) Vyas, S.; Zhang, X.; Goli, E.; Geubelle, P. H. Frontal vs. Bulk Polymerization of Fiber-Reinforced Polymer-Matrix Composites. *Compos. Sci. Technol.* **2020**, *198*, No. 108303.
(19) Nason, C.; Roper, T.; Hoyle, C.; Pojman, J. A. UV-Induced Frontal Polymerization of Multifunctional (Meth) Acrylates. *Macromolecules* **2005**, *38*, 5506−5512.
(20) Chechilo, N. M.; Enikolopyan, N. S. Structure of the Front of the Polymerization Wave and the Mechanics of Propagation of Polymerization Reaction. *Dokl. Akad. Nauk SSSR* **1974**, *214*, 1131−1133.
(21) Robertson, I. D.; Pruitt, E.; Moore, J. S. Frontal Ring-Opening Metathesis Polymerization of Exo-Dicyclopentadiene for Low Catalyst Loadings. *ACS Macro Lett.* **2016**, *5*, 593−596.
(22) Chekanov, Y. A.; Pojman, J. A. Preparation of Functionally Gradient Materials via Frontal Polymerization. *J. Appl. Polym. Sci.* **2000**, *78*, 2398−2404.
(23) Nuvoli, D.; Alzari, V.; Pojman, J. A.; Sanna, V.; Ruiu, A.; Sanna, D.; Malucelli, G.; Mariani, A. Synthesis and Characterization of Functionally Gradient Materials Obtained by Frontal Polymerization. *ACS Appl. Mater. Interfaces* **2015**, *7*, 3600−3606.
(24) Chen, S.; Tian, Y.; Chen, L.; Hu, T. Epoxy Resin/Polyurethane Hybrid Networks Synthesized by Frontal Polymerization. *Chem. Mater.* **2006**, *18*, 2159−2163.
(25) Pojman, J. A.; Craven, R.; Khan, A.; West, W. Convective Instabilities in Traveling Fronts of Addition Polymerization. *J. Phys. Chem. A* **1992**, *96*, 7466−7472.
(26) Bowden, G.; Garbey, M.; Ilyashenko, V.; Pojman, J.; Solovyov, S.; Taik, A.; Volpert, V. A. Effect of Convection on a Propagating Front with a Solid Product: Comparison of Theory and Experiments. *J. Phys. Chem. B* **1997**, *101*, 678−686.
(27) Goli, E.; Peterson, S. R.; Geubelle, P. H. Instabilities Driven by Frontal Polymerization in Thermosetting Polymers and Composites. *Composites, Part B* **2020**, *199*, No. 108306.
(28) Masere, J.; Stewart, F.; Meehan, T.; Pojman, J. A. Period-Doubling Behavior in Frontal Polymerization of Multifunctional Acrylates. *Chaos* **1999**, *9*, 315−322.
(29) Cardarelli, S. A.; Golovaty, D.; Gross, L.; Gyrya, V.; Zhu, J. A Numerical Study of One-Step Models of Polymerization: Frontal versus Bulk Mode. *Phys. D* **2005**, *206*, 145−165.
(30) Comissiong, D. M. G.; Gross, L.; Volpert, V. A. Nonlinear Dynamics of Frontal Polymerization with Autoacceleration. *J. Eng. Math.* **2005**, *53*, 59−78.
(31) Inamdar, S. R.; Pujari, N. S.; Karimi, I. A.; Ponrathnam, S.; Tayal, R. K.; Kulkarni, B. D. Spinning Wave Motion in Frontal Polymerization. *Chem. Eng. Sci.* **2007**, *62*, 1448−1455.
(32) Pojman, J. A.; Masere, J.; Petretto, E.; Rustici, M.; Huh, D.-S.; Kim, M. S.; Volpert, V. The Effect of Reactor Geometry on Frontal polymerization spin modes. *Chaos* **2002**, *12*, 56−65.
(33) Riolfo, L. A.; Carballido-Landeira, J.; Bounds, C. O.; Pojman, J. A.; Kalliadasis, S.; De Wit, A. Experimental Reaction-Driven Liquid Film Fingering Instability. *Chem. Phys. Lett.* **2012**, *534*, 13−18.
(34) Lloyd, E. M.; Feinberg, E. C.; Gao, Y.; Peterson, S. R.; Soman, B.; Hemmer, J.; Dean, L. M.; Wu, Q.; Geubelle, P. H.; Sottos, N. R.; et al. Spontaneous Patterning during Frontal Polymerization. *ACS Cent. Sci.* **2021**, *7*, 603−612.
(35) Ilyashenko, V. M..; Pojman, J. A. Single-Head Spin Modes in Frontal Polymerization. *Chaos* **1998**, *8*, 285−289.
(36) Poly(caprolactone). https://polymerdatabase.com/polymers/polycaprolactone.html.
(37) Fraga-López, F.; Manuel Martínez-Ageitos, J.; Rodríguez-Núñez, E.; Blanco-Mendez, J.; Luzardo-Álvarez, A.; Calvo-Carnota, E.; Jiménez-Carrillo, L. The Mechanism and Energy of Activation of the Melting of Poly (ε-caprolactone) with and without Prior Treatment with Span 80. *J. Appl. Polym. Sci.* **2011**, *121*, 3635−3640.
(38) Gaston, D.; Newman, C.; Hansen, G.; Lebrun-Grandie, D. MOOSE: A Parallel Computational Framework for Coupled Systems of Nonlinear Equations. *Nucl. Eng. Des.* **2009**, *239*, 1768−1778.

https://doi.org/10.1021/acs.jpcb.1c03899
J. Phys. Chem. B 2021, 125, 7537−7545

(39) Gao, Y.; Dearborn, M.; Hemmer, J.; Wang, Z.; Esser-Kahn, A.; Geubelle, P. Controllable Frontal Polymerization and Thermal Patterns Enabled by Phase-Changing Particles, 2020, Submitted.
(40) Chen, D. R.; Bei, J. Z.; Wang, S. G. Polycaprolactone Microparticles and Their Biodegradation. *Polym. Degrad. Stab.* **2000**, *67*, 455−459.
(41) Novozhilov, B. V. Propagation Rate of the Front of an Exothermic Reaction in Condensed Phase. *Dokl. Akad. Nauk* **1961**, *141*, 151−153.
(42) Garbey, M.; Taik, A.; Volpert, V. Linear Stability Analysis of Reaction Fronts in Liquids. *Q. Appl. Math.* **1996**, *54*, 225−247.
(43) Kumar, A.; Gao, Y.; Geubelle, P. H. Analytical estimates of front velocity in the frontal polymerization of thermoset polymers and composites. *J. Polym. Sci.* **2021**, *59*, 1109−1118.
(44) Solovyov, S. E.; Ilyashenko, V. M.; Pojman, J. A. Numerical Modeling of Self-Propagating Polymerization Fronts: The Role of Kinetics on Front Stability. *Chaos* **1997**, *7*, 331−340.
(45) Volpert, V. A.; Volpert, V.; Pojman, J. A.; Solovyov, S. E. Hydrodynamic Stability of A Polymerization Front. *Eur. J. Appl. Math.* **1996**, *7*, 303−320.
(46) Goli, E.; Gai, T.; Geubelle, P. H. Impact of Boundary Heat Losses on Frontal Polymerization. *J. Phys. Chem. B* **2020**, *124*, 6404−6411.

https://doi.org/10.1021/acs.jpcb.1c03899
J. Phys. Chem. B 2021, 125, 7537−7545